HHS Public Access

Author manuscript

Metallomics. Author manuscript; available in PMC 2019 December 12.

Published in final edited form as:

Metallomics. 2018 December 12; 10(12): 1728–1742. doi:10.1039/c8mt00133b.

Antimicrobial action of calprotectin that does not involve metal withholding†

Angelique N. Besold[#a], **Edward M. Culbertson**[#a], **Lily Nam**[a], **Ryan P. Hobbs**[a,*], **Alisa Boyko**[a], **C. Noel Maxwell**[b], **Walter J. Chazin**[b], **Adriana R. Marques**[c], and **Valeria C. Culotta**[a,#]

[a]Department of Biochemistry and Molecular Biology, The Johns Hopkins University Bloomberg School of Public Health, Baltimore, MD, USA

[b]Departments of Biochemistry and Chemistry and Center for Structural Biology, Vanderbilt University, Nashville, TN, USA

[c]Laboratory of Clinical Immunology and Microbiology, National Institute of Allergy and Infectious Disease, Bethesda, MD, USA.

[#] These authors contributed equally to this work.

Abstract

Calprotectin is a potent antimicrobial that inhibits the growth of pathogens by tightly binding transition metals such as Mn and Zn, thereby preventing their uptake and utilization by invading microbes. At sites of infection, calprotectin is abundantly released from neutrophils, but calprotectin is also present in non-neutrophil cell types that may be relevant to infections. We show here that in patients infected with the Lyme disease pathogen *Borreliella (Borrelia) burgdorferi*, calprotectin is produced in neutrophil-free regions of the skin, in both epidermal keratinocytes and in immune cells infiltrating the dermis, including CD68 positive macrophages. In culture, *B. burgdorferi*'s growth is inhibited by calprotectin, but surprisingly, the mechanism does not involve the classical withholding of metal nutrients. *B. burgdorferi* cells exposed to calprotectin cease growth with no reduction in intracellular Mn and no loss in activity of Mn enzymes including the SodA superoxide dismutase. Additionally, there is no obvious loss in intracellular Zn. Rather than metal depletion, we find that calprotectin inhibits *B. burgdorferi* growth through a mechanism that requires physical association of calprotectin with the bacteria. By comparison, calprotectin inhibited *E. coli* growth without physically interacting with the microbe, and calprotectin effectively depleted *E. coli* of intracellular Mn and Zn. Our studies with *B. burgdorferi* demonstrate that the antimicrobial capacity of calprotectin is complex and extends well beyond simple withholding of metal micronutrients.

†Electronic supplementary information (ESI) is available.

[#]To whom correspondence should be addressed vculott1@jhu.edu.
[*]Current address: Department of Dermatology, Pennsylvania State University College of Medicine, Hershey, PA, USA

CONFLICTS OF INTEREST

There are no conflicts of interest to declare.

Abstract

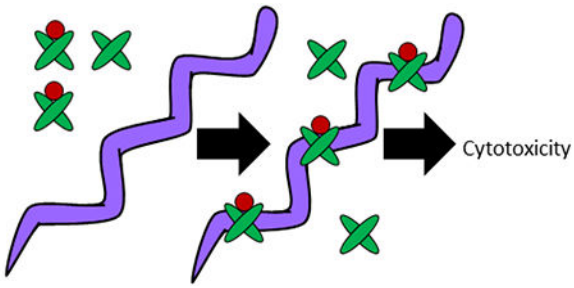

The metal (red) bound form of calprotectin (green) binds *Borrelia burgdorferi* and inhibits pathogen growth without metal withholding.

INTRODUCTION

Transition metals such as Mn, Zn, Cu and Fe are essential micronutrients for virtually all living organisms, yet these same elements are potentially toxic. During infection, the host exploits this double-edged sword as part of the immune response against invading pathogens. The host may either attack pathogens with high/toxic levels of metals or starve the invading microbe of metal micronutrients through a process called nutritional immunity.[1–3] One of the best studied examples of nutritional immunity involves calprotectin (CP), a member of the S100 family of proteins.[3] CP consists of a heterodimer of S100A8 and S100A9 proteins and has been shown to form higher order oligomers in the presence of Zn or excess calcium.[4–7] Each heterodimer binds transition metals with high affinity through two distinct metal coordinating sites at the dimer interface.[2, 3, 8, 9] Site 1 consists of six histidine residues (two from S100A8 and four from S100A9), while site 2 consists of two histidine residues from S100A8 and a histidine and aspartate from S100A9. Both sites have been shown to tightly bind Zn with affinities ranging from low nanomolar to sub-picomolar.[10–13] Unlike Zn, Mn only binds site 1 with high affinity (sub-nanomolar to low nanomolar range) [10, 11, 14, 15]; the relatively poor binding of Mn to site 2 (micromolar range) is not likely to contribute to Mn sequestration.[10, 14] Both sites are reported to bind other transition metals including Cu, Fe and Ni.[16–18] CP is an abundant component of neutrophils that is released at sites of infection in concentrations reaching 1 mg/mL.[19] With its high affinity for transition metals, CP can effectively deplete the extracellular environment of metals such as Mn and Zn, thereby starving neighboring microbes of these metal nutrients.[2, 3] CP has been reported to act as an antimicrobial for numerous bacteria[11, 12, 17, 20–27] and the mechanism has been widely ascribed to the withholding of metal nutrients. [10–12, 17, 21–24, 28–33]

As with many bacterial microbes, the Lyme disease (LD) pathogen *Borreliella (Borrelia) burgdorferi* (*Bb*) is susceptible to growth inhibition by CP *in vitro*.[20, 34] *Bb* represents a particularly interesting case of metals in biology in that the organism has uniquely evolved with no known requirement for Fe.[35, 36] Additionally, there is no known nutritional requirement for Cu, although the spirochete has evolved methods to detoxify the metal.[37] *Bb* can accumulate high levels of Mn through at least two Mn uptake systems[38, 39], and Mn acquisition is essential for pathogenesis.[39] This high Mn is required to activate a Mn

containing SodA superoxide dismutase [36, 40, 41] essential for virulence.[42] Aside from Mn, *Bb* requires Zn to activate numerous Zn metalloenzymes [43–46] and the spirochete is capable of maintaining constant Zn levels despite fluctuations in environmental Zn.[47] Based on *Bb*'s dependence on Mn and Zn micronutrients, it is possible that withholding of one or both metals accounts for this anti-*Borrelia* activity of CP, although this has never been directly tested.

As mentioned above, neutrophils are believed to be the primary source of anti-microbial CP for diverse microbial pathogens. In LD, neutrophils can play a significant role in the inflammatory response of persistent infections, particularly in joints and synovial fluid.[20, 34] However, the predominant target of *Bb* infections in both early and early disseminated stages of disease is the skin, classically presenting as the erythema migrans (EM) rash at the site of the tick bite, as well as multiple EM as a result of hematogenous dissemination of the spirochete. These rashes show little or no infiltration with neutrophils.[48, 49] However, in a transcriptome study, S100A8 and S100A9 were significantly upregulated in EM lesions.[50] Moreover, the skin is known to produce many S100 family members including S100A7, S100A12, S100A8 and S100A9, and CP is known to be secreted by keratinocytes.[51–57]

Herein, we use a combination of human tissue analyses and microbiology to explore the connection between CP and *Bb*. We provide evidence for a non-neutrophil origin of CP relevant to LD. Specifically, CP is widely apparent in the EM rashes of LD patients in both the epidermal and dermal layers of the skin. In our *in vitro* studies, CP exhibits potent anti-*Borrelia* activity in laboratory cultures, but growth inhibition occurs in the absence of any detectable metal withholding. CP inhibits *Bb* growth at relatively low doses that are ineffective in withholding either Mn or Zn micronutrients from the spirochete. Our findings support a model in which toxicity results from physical interactions between CP and the spirochete, associated with an increased susceptibility to hypotonic stress.

EXPERIMENTAL

Ethics Statement

Individuals with EM were enrolled in prospective studies (NCT00132327 and NCT00028080) approved by the Institutional Review Board at the National Institute of Allergy and Infectious Diseases. All participants were adults (at least 18 years old) who provided written informed consent.

Skin Biopsy Samples

Specimens of skin from 3 patients with EM were obtained by 4-mm punch biopsy. Specimens were obtained from the advancing border of primary EM lesions before the start of antibiotic therapy. The sample for histology was placed in 4% formaldehyde, embedded in paraffin, and stained with hematoxylin and eosin. Control skin samples were obtained from surgical specimens of anonymous patients undergoing surgery for other purposes.

Tissue slice preparation and microscopy

Sections were deparaffinized and rehydrated using successive 5 minute washes: two washes of a xylene isomer mixture (Sigma Aldrich), two of 100% ethanol (EtOH), one of 95% EtOH, 70% EtOH, 50% EtOH, ddH_2O, and 1XPBS. Slides were then placed in 10 mM sodium citrate (pH 6.0) in a polypropylene container and put in boiling water for 10 minutes. Samples were then cooled to room temperature. Slides were then rinsed with ddH_2O and then 1X PBS for 5 minutes each. Slides were blocked in 2% Normal Goat Serum (G9023–10mL Sigma), 1% Bovine Serum Albumin for 30 minutes. The highly specific anti-S100A8 antibody (GTX54721 Gene Tex)[58] was diluted 1:100 in blocking buffer. Anti-CD8 antibody (M7103 Dako) was used at a dilution of 1:50 and anti-CD68 (790–2931 Ventana) was used at a concentration of 0.4 μg/mL. A dilution of 1:50 was used for Anti-CD163 (BM4041 Acris). Slides were incubated with primary antibody overnight at 4oC prior to being washed three times in 1XPBS for 10 minutes. Secondary antibodies goat anti-rabbit 488 (ab150077 Abcam) and goat anti-mouse 594 (ab150116 Abcam) were applied at a dilution of 1:1000 for 1 hour at room temperature. Slides were then washed two times in 1XPBS for 5 minutes each before being stained with DAPI for 5 minutes. Slides were washed once in 1XPBS for 5 minutes before being mounted on with a coverslip using FlourSave Reagent (Calbiochem). Images were taken on a Zeiss AxioObserver Z1 with Apotome microscope at 20× magnification. Larger images (Fig. S1, ESI†) were imaged at 10× and stitched together. Multiple images (approximately 10) from a single section of each sample were analyzed for S100A8 quantification. Cell counts were quantified using ImageJ. For quantification, TIFF files exported from Zeiss ZEN software were converted to 8-bit greyscale. Contrast was enhanced 5%. Pictures were thresholded to 35 before the colors were adjusted to RGB and the channels were merged. Multiple images (approximately 10) from a single section of each sample were analyzed for S100A8 quantification. A one-way ANOVA with Tukey post-test was applied. Analysis was carried out in Graphpad Prism v5.0 Software.

Bacterial strains, growth medium and growth conditions

Bb strain 297[59] and *E. coli* strain DH5α were cultured in BSK II medium (pH 7.6) containing 6% (v/v) rabbit serum [60, 61]. *E. coli* was chosen for comparative analyses based on its documented susceptibility towards metal withholding effects of CP[11, 12, 17, 32], its well-defined Mn and Fe containing superoxide dismutase enzymes[36, 62] and its ready availability as a BSL1 laboratory organism. *Bb* cultures were supplemented with 0.05 mg/mL rifampicin, 0.1 mg/mL phosphomycin, and 5 μg/mL amphotericin[61], and were maintained at 34°C; growth was monitored by counting spirochetes under dark field microscopy (Nikon Eclipse 80i). *E. coli* was cultured without antibiotics at 37°C and growth monitored by absorbance at 600 nm.

For CP toxicity studies, triplicate 200 μl cultures of *Bb* were inoculated at 1×104 cells/mL in 96-well flat-bottom plates in 80% BSK II medium with 6% rabbit serum/20% calprotectin buffer (20 mM Tris pH 7.5, 100 mM NaCl,10 mM BME, 3 mM $CaCl_2$) containing human recombinant WT or mutant CP. The metal content of this medium is shown in Table S1 (ESI†). Mn and Zn levels are similar to that of the Tryptic Soy Broth (TSB) based media previously used in studies of microbial toxicity to CP[11, 12, 17, 32] , and the levels of calcium are sufficient to activate CP.[12, 14, 17] The presence of BME does not affect cell growth in

BSK II medium. Cells were enumerated following 6–7 days of growth. *E. coli* sensitivity towards CP was tested similarly using cells inoculated at 1×107 cells/mL and grown for 5–6 hours. In both cases, cell reached late log phase growth following 7–9 cell doublings in the presence of CP. Preparative *Bb* cultures for biochemical analyses were seeded at 1×105 cells/mL; CP was added when cultures reached ≈5×105 cells/mL and growth proceeded until untreated controls reached 107–108 cells/mL. Cultures of *E. coli* for biochemical analyses were seeded in BSK II at 8×107 cells/mL and grown to ≈2 × 109 cells/mL.

Biochemical analysis

All samples of recombinant WT and mutant CP were prepared according to our standard published protocols.[10, 11] *Bb* or *E. coli* cells for biochemical analyses were harvested by centrifugation at 3,000 × g at 4°C for 50 or 20 minutes, respectively. Cell pellets were washed twice in either cold 1 mM Tris, 10 mM EDTA, pH 7.8 or in *Bb* washing buffer (20mM HEPES, pH 7.6, 100mM NaCl, 10mM EDTA)[35] followed by washing twice in cold MilliQ water. The nature of washing did not alter the level of CP associated with *Bb*. For metal analysis of *Bb* by ICP-MS, pellets containing 2×108–1×109 cells were resuspended in 500 μL of 67–70% (v/v) nitric acid (J.T. Baker, Ultrex II Ultrapure Reagent) and heated at 80°C for 1 hour. Cell debris was removed by centrifugation at 20,000 × g for 5 minutes and the supernatant was diluted 1:14 in MilliQ water prior to analysis by ICP-MS in semi-quantative mode (Agilent 7700×, University of Maryland, School of Pharmacy, Mass Spectrometry Center). With *E. coli*, 6×109–1×1010 cells were digested in 500 μL of 20% (v/v) nitric acid overnight at 90°C and diluted 1:10 in MiliQ water in preparation for ICP-MS as described above. As blank controls, BSK II medium (no cells) was incubated in parallel and subjected to the identical centrifugation, washing and acid treatments. Any metal values of these blanks were subtracted from cell samples.

For analysis of metals in the growth media, 200 μL of media (80% BSK II medium/20% calprotectin buffer with 3 mM $CaCl_2$) was digested in 1.5 mL of 23% nitric acid for 18 hours at 80°C. Digested samples were diluted to a final volume of 5.5 mL with MiliQ water (~6% final nitric acid concentration), clarified by centrifugation at 4,000 × g for 10 minutes and subjected to ICP-MS as described above. Alternatively, BSK II medium was made 1% in nitric acid and analyzed directly without dilution using an Agilent 7500ce ICP-MS (Johns Hopkins NIEHS Center Core Facility). The metal values representing 80% BSK, 20% 3 mM $CaCl_2$ were similar in the two experiments, and averages over the two trials are presented in Table S1 (ESI†).

For preparation of *Bb* and *E. coli* cell lysates, 1×108–8×1010 and 3×109–1×1010 cells, respectively, were lysed by glass bead homogenization in 150 μL of lysis buffer (10 mM potassium phosphate (KPi) pH 7.8, 5 mM EDTA, 5 mM EGTA, 50 mM NaCl, 0.45% Tergitol-type NP-40 (NP40), 10% glycerol) containing a volume of Zirconium oxide (0.7 mm) or glass (400–600 nm) beads equivalent to the cell pellet. Following vortexing at 3200 RPM for three 3 min cycles, lysates were clarified by centrifugation at 20,000 × g and stored in −80°C.

Denaturing gel electrophoresis on NuPage 4–12% BisTris Gels (Life Technologies) used ≈ 30 μg of protein lysate or 100–500 ng of recombinant CP. Gels were subjected to either

Coomassie Brilliant Blue staining or immunoblot analysis using anti-S100A9 antibody (Abcam ab63818) diluted 1:1,000 and Alexa Fluor 680 donkey anti-rabbit secondary (Life Technologies) diluted 1:10,000. To define the molar quantity of CP versus moles of Zn associated with *Bb*, a cell sample of verified Zn content (as determined by ICP-MS) was subjected to electrophoresis and Coomassie staining against known quantities of purified recombinant human CP. CP bands were quantified using ImageJ software and analyzed against the standard curve of recombinant CP.

For SOD activity, 30 to 50 μg of protein lysate was subjected to native gel electrophoresis at 50 mA using 10 or 12% Tris-glycine native gels (Novex). SOD activity was monitored by nitroblue tetrazolium (NBT) staining and Fe-SOD activity eliminated by treating gels with 30 mM H_2O_2 prior to NBT staining as described.[36]

For all *in vitro* studies, data were considered statistically significantly different for p values of ≤0.05 using the two-tailed t test as determined by Graphpad Prism v7.

Microscopy of *Bb*

For examination of *Bb* morphology, cells were examined under dark field microscopy at 40× magnification. Zinquin-dependent fluorescence was monitored by microscopy of *Bb* cells essentially as described.[43] 5×107 *Bb* cells were harvested by centrifugation at 1,000 × g for 10 minutes. Cells were washed twice with HN Buffer (20 mM NaCl, 50 mM HEPES, pH 7.6), resuspended in 500 μL HN buffer and incubated at room temperature for 5 minutes. A 5 mM stock of zinquin ethyl ester (Sigma) dissolved in DMSO was diluted 1:2 in HN buffer and added to cells at a final concentration of 25 μM followed by incubation at 34°C for 30 minutes. Cells were subsequently stained with PKH26 Red Fluorescent dye for membranes (Sigma) using 2 μL of dye diluted according to manufacturer's specifications followed by incubation for 5 minutes at room temperature. The staining was terminated by the addition of 500 μL BSK II medium. Cells were subsequently washed twice in HN Buffer, resuspended in 100 μL HN buffer and subjected to 40× fluorescence microscopy and imaging using a Zeiss Observer.Z1 microscope equipped with an Apotome VH optical sectioning grid.

RESULTS

Non-neutrophil origins of CP at sites of *Bb* infection

In cases where CP is reported to withhold metals from microbes, the host cell source is largely believed to be neutrophils.[10, 21, 22, 63] However, the primary site of infection with *Bb*, namely the EM rash in the skin, appears devoid of these immune cells.[48, 49] To determine if *Bb* may be exposed to non-neutrophil sources of CP in the skin, we analyzed sections of skin biopsies taken from the site of EM rashes from Lyme disease (LD) patients in comparison to the skin of control patients (non-LD surgical controls). As seen in the immunofluorescent microscopy images of skin in Fig. S1 (ESI†) and in the enlarged images of Fig. 1, variable staining with a S100A8 antibody was seen in individual cells of the epidermis (defined by DAPI staining), where one LD patient (patient C) had particularly high epidermal S100A8. Upon quantification of multiple images, there was no major

difference between S100A8 positive epidermal cells in the EM rash of LD patients versus the skin of controls (Fig. 2A). *Bb* is known to colonize the dermal layer of skin[64], and we observed punctate staining of S100A8 in specific dermal cells of all three patients (Fig. 1). This precise pattern of punctate dermal staining for CP has been previously noted in cases of skin inflammation and wound healing.[53, 65–67] Upon quantification, the total number of S100A8 positive cells in the dermal layer varied among the individuals (Fig. 2B), although there was a trend towards increased S100A8 positive cells in the skin of LD patients compared to controls (see legend to Fig. 2B).

The epidermal staining of S100A8 is likely keratinocytes, which comprise approximately 95% of cells within the epidermis[68], and these cells are well known to produce and secrete CP.[51, 52, 69] By contrast, the nature of the dermal staining was unclear. The EM rash of LD patients is devoid of neutrophils [48, 49, 70], but is marked with infiltrating lymphocytes and occasional macrophages.[71] Macrophages can produce CP [2, 72–74], and in other reports of inflammation (non-LD), CD68 positive macrophages and CD8 positive lymphocytes have been shown to express CP.[74, 75] We observed both of these immune cell markers in the dermis of LD patients (Figs. 3 and 4 and Tables 1 and 2). In double labeling studies, the LD patient with the lowest dermal S100A8 (patient A) showed negligible co-localization of S100A8 with either CD8 or CD68 markers (Figs. 3 and 4; Tables 1 and 2). By comparison, the two patients with high dermal S100A8 (patients B and C) showed marked (25–40%) co-localization of S100A8 with the macrophage CD68 marker (Fig. 4 and Table 2). There was also some co-localization of S100A8 with CD8, but the cells numbers were comparatively low and restricted to patient B (Fig. 3 and Table 1). It is important to note that a fraction of S100A8 positive cells were neither positive for CD68 nor CD8 and analysis of other immune markers such as CD163 proved negative (Fig. S2, ESI†). Additional cell types currently of unknown nature must contribute to CP in the infected dermis (see Discussion). Regardless of the nature of these cells, our studies demonstrate that CP can exist at sites of primary *Bb* infection in the skin, even in the absence of neutrophils, providing evidence that CP may be important for fighting *Bb* at the site of infection.

CP effects on *Bb* growth in culture and *Bb* metals

We next addressed how CP impacts *Bb* growth and metal homeostasis using laboratory cultures of the spirochete and recombinant human CP. Growth of *Bb* in laboratory cultures requires a specialized medium (BSK II) rich in rabbit serum and albumin, whereby the spirochete grows optimally between 30oC – 37oC and doubles once every 12–24 hours[60, 76]. Consistent with previous studies[20, 34], *Bb* growth is strongly inhibited by CP at concentrations greater than 100 μg/mL (Fig. 5A). These levels of CP are significantly lower than what has been reported for several other bacteria grown in different media including *Helicobacter pylori*[30], *Staphylococcus sp, Pseudomonas aeruginosa* and *Escherichia coli*.[11], but within the range for other organisms including *Listeria monocytogenes*, *Streptococcus mutans* [33] and *Candida albicans*.[77] To determine if the BSK II medium affects the bioactive dose of CP, *E. coli* susceptibility to CP was examined in this serum rich medium. As seen in Fig. 5B, growth of *E. coli* grown in BSK II is inhibited by >0.5 mg/mL CP, nearly five times the toxic dose of CP for *Bb* grown in BSK II (Fig. 5A). Thus, *Bb* seems to have a particularly high sensitivity to growth inhibition by CP, at least compared to *E. coli*.

CP can sequester transition metals using two high affinity metal binding sites and we tested whether this metal binding property was important for the *Bb* growth inhibition observed. To accomplish this, we used a mutant of CP, termed ΔS1ΔS2, that lacks transition metal binding capabilities. Specifically, four of the six metal coordinating histidines of site 1 were mutated to asparagine and the three histidines and single aspartic acid of metal binding site 2 were mutated to asparagine and serine, respectively.[11] As seen in Fig. 6A, this ΔS1ΔS2 CP mutant showed no toxicity to *Bb*. Additionally, we examined the effects of individual mutations at site 1 versus site 2 and find that CP toxicity was also greatly reversed with ΔS2 CP mutated at site 2 (Fig. 6B). By comparison, ΔS1 CP defective in site 1 effectively attenuated *Bb* growth at 125 μg/mL, similar to WT CP (Fig. 6B), although ΔS1 CP did show some loss of toxicity at the lower dose of 80 μg/mL. Thus, of the two metal binding sites, site 2 appears most critical for inhibiting *Bb* growth in culture, with site 1 contributing less to toxicity.

Mn binds to CP specifically through site 1 and since the ΔS1 mutant is still toxic to *Bb*, this suggests that CP does not inhibit the growth of *Bb* by withholding Mn. To investigate this, we examined total Mn levels in *Bb* by ICP-MS. As seen in Fig. 7A, there was no decrease in Mn in *Bb* cells cultured at the mean inhibitory concentration (MIC) of CP (80 μg/mL). If anything, Mn levels rose (Fig. 7A). We also examined activity of the Mn dependent superoxide dismutase SodA, a biomarker of intracellular Mn in *Bb*.[36, 40, 42] Although the equivalent SodA in *Staphylococcus aureus* is inactivated by CP in culture [10, 29], we observed no such inhibition of SodA in *Bb* when cells were cultured (Fig. 7B). Altogether, the findings of Fig. 6B, 7A and 7B demonstrate that CP inhibits *Bb* growth without withholding Mn from the bacteria.

In complex growth media such as BSK II, the binding of metals to CP is affected by the relative bioavailability of the transition metals Mn, Zn, Cu and Fe. As seen in Table S1 (ESI†), and consistent with previous findings[47], BSK II media contains Mn and Zn levels that approximate that of the TSB-based medium employed in earlier studies involving CP. [11, 12, 17, 32] However, Fe and Cu are higher in BSK II, with contributions from serum (e.g., heme, ferritin, transferrin and cupro-ceruloplasmin) and albumin[78–80]. It was therefore possible that the lack of Mn withholding by CP was due to poor availability of Mn compared to these other metals. To address this possibility, we used *E. coli* as an indirect approach to monitoring CP sequestration of metals from BSK II. *E. coli* is reportedly susceptible to metal withholding by CP [11, 17, 32], and any loss in *E. coli* Mn would be indicative of CP binding to Mn in BSK II. As seen in Fig. 7C, CP treatment of *E. coli* resulted in a pronounced decrease in intracellular Mn, at both the 80 μg/mL mean inhibitory dose for *Bb* and at the higher 350 μg/mL dose that approximates the mean inhibitory dose for *E. coli*. This lowering of intracellular Mn in *E. coli* impacted Mn availability for SOD enzymes. Like *Bb, E. coli* expresses a Mn dependent SodA in addition to an Fe containing SodB. These SODs can be discerned by differential sensitivity towards H_2O_2 inactivation (Fig. 7D).[36] As seen in Fig. 7E, the activity of the Mn requiring SodA was greatly attenuated in BSK II cultures treated with CP, even at the 80 μg/mL dose, which has no effect on the activity of *Bb* SodA (Fig. 7B). In spite of potentially competing Fe, Cu and Zn ions, CP has the capacity to sequester Mn in BSK II medium. However, *Bb* seems refractory to this Mn sequestration by CP.

Rather than Mn, CP may withhold Zn from *Bb*. In fact, Montgomery and colleagues reported reversal of CP toxicity in *Bb* cultures treated with 3 μM Zn, suggestive of Zn withholding.[20] However, we failed to observe any reversal of CP toxicity with similar Zn supplements (Fig. S3A, ESI†) and Zn supplements up to 25 μM (BSK II has ≈3 μM Zn, Table S1, ESI†) did not change the mean inhibitory concentration of CP towards *Bb* (Fig. S3B, ESI†). To directly test whether CP withholds Zn from *Bb*, we measured total Zn in the spirochete by ICP-MS. As seen in Fig. 8A, there was no diminution in Zn in *Bb* when cultured with the mean inhibitory dose of CP. In fact, Zn levels dramatically rose >10 fold. A similar rise was seen with Cu, while Fe levels were below limits of detection with or without CP treatment (Fig. S4A). By comparison, *E. coli* cultured at its mean inhibitory dose of 350 μg/mL CP exhibited a striking decrease in intracellular Zn (Fig. 8B). At the lower 80 μg/mL dose of CP that is non-toxic to *E. coli*, there was no withholding of Zn and, if anything, Zn levels slightly rose, although this was minor (≈50%) (Fig 8B). The growth inhibition of *E. coli* by high levels of CP (350 μg/mL) clearly correlates with CP withholding of both Mn and Zn. Additionally, we observed withholding of *E. coli* Fe and Cu micronutrients at this mean inhibitory concentration of CP (Fig. S4B,C, ESI†) and a decrease in Fe-SodB activity (Fig 7E). This loss of Fe and Cu micronutrients for *E. coli* may also contribute to the growth inhibition. Compared to these effects on *E. coli*, CP inhibits *Bb* growth at lower doses and in the absence of any obvious withholding of the metal nutrients for *Bb*, Mn and Zn.

CP interactions with *Bb*

In cases where CP withholds metals from microbes, metal depletion can be accomplished without physically contacting the organism, examples including *S. aureus, Streptococcus pyogenes, Streptococcus pneumoniae* and the fungal pathogen *C. albicans*.[21, 25, 81] CP simply acts by modifying the extracellular environment through metal sequestration. However, there are rare reports of CP directly interacting with microbes, e.g., *Neisseria* species and *Finegoldia magna* [25, 82, 83]. We investigated whether the same is true for *Bb*. As seen in Fig. 7B, bottom panel, a doublet protein of ≈11–13 kDa was evident in whole cell lysates of CP treated *Bb* cells, but not in lysates from control untreated *Bb*. Upon closer inspection, this doublet was seen to co-migrate with S100A8 (10.8 kDa) and S100A9 (13.2 kDa) subunits of CP (Fig. 9A, left panel), and the 13 kDa species cross-reacted with an anti-S100A9 antibody on immunoblots (Fig. 9A, right panel). The appearance of CP in whole cell lysates of *Bb* did not reflect non-specific precipitation or aggregation of the protein, as CP was retained following extensive washing of *Bb* cells (see Experimental) and required the presence of *Bb* cells. As seen in Fig. 9B, CP was undetectable in lysates of *E. coli* cultured in the same BSK II medium, despite higher levels of CP used to treat *E. coli* (350 μg/mL) versus *Bb* (80 μg/mL).

We next tested whether CP association with *Bb* required transition metal binding sites 1 and/or 2. As seen in Fig. 9C top and middle panels, the ΔS2 and ΔS1ΔS2 mutants of CP were absent in lysates of *Bb*, despite equivalent amounts of CP protein added to the culture (Fig. 9C bottom). The only CP mutant recovered in *Bb* cell lysates was ΔS1 CP, although the level of CP recovered with the ΔS1 mutant was less than that of WT CP. Together these results demonstrate that CP interactions with *Bb* relies heavily on site 2, and to a lesser

extent, on site 1. It is noteworthy that these results completely parallel findings with CP toxicity where growth inhibition is strongly dependent on site 2, and partly dependent on site 1 (Fig. 6B). Thus, toxicity against *Bb* is dependent on the ability of CP to physically associate with the spirochete.

Microscopy analyses of intracellular Zn and *Bb* morphology with CP treatment

Since CP is abundantly recovered with *Bb*, it was possible that the aforementioned elevation in *Bb* Zn (Fig. 8A) could be attributable to Zn bound to CP. In fact, we observed a near stoichiometric ratio of *Bb*-associated CP versus the rise in *Bb*-associated Zn (e.g., 30 nmoles CP/109 cells versus 32 nmoles Zn/109 cells, see Experimental). If the Zn measured by ICP-MS is largely bound to CP, it remained possible that CP was in fact depleting Zn bioavailability inside *Bb* cells. To address this, we employed the fluorescent Zn probe zinquin, which was previously used by Gherardini and colleagues to tract available Zn in *Bb*.[43] Zinquin has an affinity constant for Zn in the nanomolar range and is believed to report on loosely bound or accessible Zn pools.[8485] To validate zinquin as a reporter for *Bb* Zn, we used the metal chelator TPEN (*N*,*N*,*N*′,*N*′-tetrakis(2-pyridylmethyl ethylenediamine), which has an affinity constant for Zn in the femtomolar range.[86] *Bb* cells were grown with relatively non-toxic levels of 3 μM TPEN (Fig. S5, ESI†) followed by staining with zinquin and the PKH red dye for whole cell membranes. As seen in Fig. 10A, zinquin fluorescence in *Bb* was greatly diminished in TPEN cultured cells. By comparison, there was no detectable loss in zinquin fluorescence in cells cultured at the mean inhibitory dose of CP (Fig. 10B). This finding supports the notion that CP inhibits *Bb* growth through a mechanism that does not involve Zn starvation.

How can the growth of *Bb* be inhibited? Several agents that inhibit *Bb* growth, such as certain antibiotics or other stress conditions, can induce the morphological cyst-like states known as ‘round bodies” or ‘blebs’.[87–90] The round body consists of a spherical membrane-bound structure, while a bleb, which may be an intermediate between the spirochete and round body, consists of a short spirochete with a terminal rounded structure.[90] These cyst forms have decreased metabolic activity, potentially as a means to enhance survival, but have the ability to revert to the spirochete in the absence of the stressor. [88, 90] We observed that when growth was inhibited by CP, *Bb* retained its characteristic spiral spirochete conformation (Fig. 10B and11A left) by dark field microscopy. However, upon immediate dilution by 10-fold in water, CP treated cells rapidly converted into blebs, as well as occasional round bodies (Fig. 11A right, 11B). The control cells not treated with CP remained in the elongated spiral spirochete conformation under the same short exposures to hypotonic conditions (Fig. 11), consistent with findings by Alban *et al.*[88] Rapid conversion to cysts with CP treated *Bb* was seen in cultures diluted in water, but not with cells diluted in phosphate buffer saline (Fig. S6, ESI†). We conclude that CP interactions with *Bb* affects the spirochete in a manner that increases sensitivity towards hypotonic stress (see Discussion).

Altogether, the *in vitro* culture studies demonstrate that CP inhibits *Bb* growth through a mechanism that does not involve the traditional withholding of Mn and Zn micronutrients as

has been described for other microbes. Instead, CP physically interacts with the *Bb* spirochete and results in an increased propensity for *Bb* cyst formation.

DISCUSSION

The canonical mode of action of CP in fighting pathogens involves withholding essential metal micronutrients. In the case of *Bb*, CP exerts its antimicrobial effects without starving the pathogen of Zn and/or Mn micronutrients. Here we provide an example of where CP inhibits bacterial growth without any obvious effects on metal accumulation. In fact, *Bb* appears to be particularly resilient to the Mn withholding effects of CP, at least compared to *E. coli* examined under parallel conditions. *Bb* expresses at least two Mn uptake systems [38, 39] and is capable of accumulating high levels of Mn that are needed to support SodA activity.[36, 40] The low level of CP that inhibits *Bb* growth may not adequately compete with the *Bb* uptake systems for accumulating Mn, even though this level of CP effectively competes with the Mn uptake systems of *E. coli*. Like *Bb, Salmonella* and *S. aureus* have been shown to be resistant to CP mediated Mn depletion through the use of strong Mn uptake systems.[28, 63] *Bb* may use potent metal uptake systems for both Mn and Zn to combat metal depletion by CP.

Typically, CP acts at a distance to deplete extracellular metals, but the anti-*Bb* activity of CP involves the direct association of the protein with the bacteria. Examples of CP directly interacting with bacterial microbes are rare. In certain strains of the bacterial pathogen *Finegoldia magna*, CP binds to a surface protein called protein L that protects the cell from the anti-microbial effects of CP. In *F. magna* strains that lack protein L, CP associates with the membrane and causes cell wall/membrane disintegration.[25] Interestingly, *Neisseria sp* bind metal bound CP through the CpbA receptor and use this CP as a nutrient Zn source. [82, 83] *Bb* does not express orthologues of protein L or CpbA and the mechanism of the CP-*Bb* interactions is not understood. In addition to bacteria, CP and other S100 proteins can bind directly to certain parasitic species. CP has been shown to interact with the surface of adult *Onchocerca volvulus* and with *Echinococcus granulosus*, although it remains unclear how this affects the growth of the worms.[91, 92] In addition to CP, the related Zn binding S100A12 protein physically interacts with both *O. volvulus*[93] and the nematode *Brugia malayi*.[94, 95] As is the case with CP and *Bb*, S100A12 inhibits the growth of *B. malayi* without metal withholding. Rather, S100A12 binding to the parasite disrupts the contractile elements, affecting worm motility.[94, 95] Overall these studies with parasitic worms and the spirochete *Bb* suggest that CP can inhibit pathogen growth through mechanisms that involve physical interactions with the microbe, not metal withholding. In the case of *Bb*, our studies do not discern between CP binding strictly to the cell surface versus CP uptake into the cell. We consider the latter possibility unlikely as other cases of CP interactions with microbes involve cellular membranes [25, 82, 83].

How does the interaction with CP inhibit *Bb* growth? Since growth inhibition tracks with an increased sensitivity towards hypotonic conditions, one possibility is that CP may somehow affect the membrane, as evidenced by *Bb* cyst formation upon immediate dilution in water. Although such hypotonic conditions are not likely to be encountered *in vivo*, the osmotic sensitivity observed *in vitro* may be indicative of issues with membrane or osmolyte balance.

Regardless of the mechanism, the physical association of CP with *Bb* seems to require metals, such as Zn, Mn, Cu, and Fe, as intact metal binding sites are necessary for CP-*Bb* interactions. Moreover, the binding of CP to *Bb* correlates with high levels of Zn and Cu that associate with the microbe, presumably reflecting Zn-CP and Cu-CP bound to *Bb* (Figs. 8A and S4A). Therefore, we propose the following model: CP binds to transition metals, helping to stabilize CP and/or induce its tetramerization, as has been shown for Zn.[4] Metal binding to site 2, and to a lesser extent, site 1, then promotes CP association with *Bb*, although it is currently unknown if this association is through the cell membrane of if CP is internalized. Once associated, CP may affect the membrane in a way that inhibits microbial growth in the absence of metal withholding. Additional studies are required to define the role of each metal site in promoting CP interactions with *Bb* as well as determine the molecular targets in *Bb* that account for CP binding and growth inhibition.

When does *Bb* encounter CP *in vivo*? With persistent infections, where *Bb* accumulates in joints and synovial fluid, the spirochete is likely to encounter CP secreted by infiltrating neutrophils.[20, 34] In the skin, a primary organ of *Bb* infection, there is no infiltration of neutrophils; however, we show here that a non-neutrophil source of CP is prevalent in the EM rash. We observe cells expressing S100A8 in keratinocytes of the epidermis as well as scattered S100A8 producing cells of dermal layer. Keratinocytes are well known to secrete CP [51–54] and a punctate pattern of dermal S100A8 staining has also been observed in other cases of skin inflammation and wound healing, although the nature of these specific dermal cells was unclear.[53, 65–67] We have identified a defined number of dermal CP positive cells as CD68 expressing monocytes/macrophages. Although the level of CP produced by these cells in the skin may not be as high as that derived from neutrophils, *Bb* is sensitive to much lower doses of CP compared to other bacteria. When the antimicrobial action of CP involves metal withholding, very high levels of CP are required to deplete the extracellular environment of Zn and/or Mn. By comparison, much lower doses of CP can inhibit *Bb* growth by physically interacting with the microbe without the need to modify the bioavailability of environmental metals.

CONCLUSION

CP is known to inhibit the growth of diverse microbial pathogens by withholding metal micronutrients and this mechanism of antimicrobial activity has become near dogmatic. Here, we provide evidence for the first time that this protein can inhibit bacterial growth without starving the microbe of essential metals. The capacity of CP to act as an antimicrobial is indeed complex and depending on the microbe and host niche, circumstances beyond nutritional immunity should considered.

Supplementary Material

Refer to Web version on PubMed Central for supplementary material.

ACKNOWLEDGEMENTS

We thank Sarah Attreed for help with *Bb* toxicity studies and Pierre Coulombe for helpful discussion. This research was supported by the Global Lyme Alliance (VCC), by NIH grants RO3 AI109297 (VCC), R01 AI101171 (WJC),

R01 AR044232 (RPH), F32 AI124506 (ANB), and F31 DK111114–01 (EMC), and by the Intramural Research Program of the NIH, National Institute of Allergy and Infectious Diseases.

REFERENCES

1. Hood MI and Skaar EP, Nutritional immunity: transition metals at the pathogen-host interface, Nat. Rev. Microbiol, 2012, 10, 525–537. [PubMed: 22796883]
2. Zackular JP, Chazin WJ and Skaar EP, Nutritional Immunity: S100 Proteins at the Host-Pathogen Interface, J. Biol. Chem, 2015, 290, 18991–18998. [PubMed: 26055713]
3. Zygiel EM and Nolan EM, Transition Metal Sequestration by the Host-Defense Protein Calprotectin, Annu. Rev. Biochem, 2018, 87, 621–643. [PubMed: 29925260]
4. Vogl T, Leukert N, Barczyk K, Strupat K and Roth J, Biophysical characterization of S100A8 and S100A9 in the absence and presence of bivalent cations, Biochim. Biophys. Acta, 2006, 1763, 1298–1306. [PubMed: 17050004]
5. Strupat K, Rogniaux H, Van Dorsselaer A, Roth J and Vogl T, Calcium-induced noncovalently linked tetramers of MRP8 and MRP14 are confirmed by electrospray ionization-mass analysis, J. Am. Soc. Mass Spectrom, 2000, 11, 780–788. [PubMed: 10976885]
6. Vogl T, Roth J, Sorg C, Hillenkamp F and Strupat K, Calcium-induced noncovalently linked tetramers of MRP8 and MRP14 detected by ultraviolet matrix-assisted laser desorption/ionization mass spectrometry, J. Am. Soc. Mass Spectrom, 1999, 10, 1124–1130. [PubMed: 10536818]
7. Stephan JR and Nolan EM, Calcium-induced Tetramerization and Zinc Chelation Shield Human Calprotectin from Degradation by Host and Bacterial Extracellular Proteases, Chem. Sci, 2016, 7, 1962–1975. [PubMed: 26925211]
8. Gilston BA, Skaar EP and Chazin WJ, Binding of transition metals to S100 proteins, Sci. China Life Sci, 2016, 59, 792–801. [PubMed: 27430886]
9. Cunden LS and Nolan EM, Bioinorganic Explorations of Zn(II) Sequestration by Human S100 Host-Defense Proteins, Biochemistry, 2018, DOI: 10.1021/acs.biochem.7b01305.
10. Kehl-Fie TE, Chitayat S, Hood MI, Damo S, Restrepo N, Garcia C, Munro KA, Chazin WJ and Skaar EP, Nutrient Metal Sequestration by Calprotectin Inhibits Bacterial Superoxide Defense, Enhancing Neutrophil Killing of *Staphylococcus aureus*, Cell Host Microbe, 2011, 10, 158–164. [PubMed: 21843872]
11. Damo SM, Kehl-Fie TE, Sugitani N, Holt ME, Rathi S, Murphy WJ, Zhang Y, Betz C, Hench L, Fritz G, Skaar EP and Chazin WJ, Molecular basis for manganese sequestration by calprotectin and roles in the innate immune response to invading bacterial pathogens, Proc. Natl. Acad. Sci. U. S. A, 2013, 110, 3841–3846. [PubMed: 23431180]
12. Brophy MB, Hayden JA and Nolan EM, Calcium ion gradients modulate the zinc affinity and antibacterial activity of human calprotectin, J. Am. Chem. Soc, 2012, 134, 18089–18100. [PubMed: 23082970]
13. Nakashige TG, Stephan JR, Cunden LS, Brophy MB, Wommack AJ, Keegan BC, Shearer JM and Nolan EM, The Hexahistidine Motif of Host-Defense Protein Human Calprotectin Contributes to Zinc Withholding and Its Functional Versatility, J. Am. Chem. Soc, 2016, 138, 12243–12251. [PubMed: 27541598]
14. Hayden JA, Brophy MB, Cunden LS and Nolan EM, High-affinity manganese coordination by human calprotectin is calcium-dependent and requires the histidine-rich site formed at the dimer interface, J. Am. Chem. Soc, 2013, 135, 775–787. [PubMed: 23276281]
15. Hadley RC, Gagnon DM, Brophy MB, Gu Y, Nakashige TG, Britt RD and Nolan EM, Biochemical and Spectroscopic Observation of Mn(II) Sequestration from Bacterial Mn(II) Transport Machinery by Calprotectin, J. Am. Chem. Soc, 2018, 140, 110–113. [PubMed: 29211955]
16. Besold AN, Gilston BA, Radin JN, Ramsoomair C, Culbertson EM, Li CX, Cormack BP, Chazin WJ, Kehl-Fie TE and Culotta VC, The role of calprotectin in withholding zinc and copper from *Candida albicans*, Infect. Immun, 2018, 86, e00779–00717.
17. Nakashige TG, Zhang B, Krebs C and Nolan EM, Human calprotectin is an iron-sequestering host-defense protein, Nat. Chem. Biol, 2015, 11, 765–771. [PubMed: 26302479]

18. Nakashige TG, Zygiel EM, Drennan CL and Nolan EM, Nickel Sequestration by the Host-Defense Protein Human Calprotectin, J. Am. Chem. Soc, 2017, 139, 8828–8836. [PubMed: 28573847]
19. Clohessy PA and Golden BE, Calprotectin-mediated zinc chelation as a biostatic mechanism in host defence, Scand. J. Immunol, 1995, 42, 551–556. [PubMed: 7481561]
20. Lusitani D, Malawista SE and Montgomery RR, Calprotectin, an abundant cytosolic protein from human polymorphonuclear leukocytes, inhibits the growth of *Borrelia burgdorferi*, Infect. Immun, 2003, 71, 4711–4716. [PubMed: 12874352]
21. Corbin BD, Seeley EH, Raab A, Feldmann J, Miller MR, Torres VJ, Anderson KL, Dattilo BM, Dunman PM, Gerads R, Caprioli RM, Nacken W, Chazin WJ and Skaar EP, Metal chelation and inhibition of bacterial growth in tissue abscesses, Science, 2008, 319, 962–965. [PubMed: 18276893]
22. Gaddy JA, Radin JN, Loh JT, Piazuelo MB, Kehl-Fie TE, Delgado AG, Ilca FT, Peek RM, Cover TL, Chazin WJ, Skaar EP and Scott Algood HM, The host protein calprotectin modulates the Helicobacter pylori cag type IV secretion system via zinc sequestration, PLoS Pathog., 2014, 10, e1004450. [PubMed: 25330071]
23. Hood MI, Mortensen BL, Moore JL, Zhang Y, Kehl-Fie TE, Sugitani N, Chazin WJ, Caprioli RM and Skaar EP, Identification of an Acinetobacter baumannii zinc acquisition system that facilitates resistance to calprotectin-mediated zinc sequestration, PLoS Pathog., 2012, 8, e1003068. [PubMed: 23236280]
24. Miyasaki KT, Bodeau AL, Murthy AR and Lehrer RI, In vitro antimicrobial activity of the human neutrophil cytosolic S-100 protein complex, calprotectin, against *Capnocytophaga sputigena*, J. Dent. Res, 1993, 72, 517–523. [PubMed: 8423249]
25. Akerström B and Bjorck L, Bacterial surface protein L binds and inactivates neutrophil proteins S100A8/A9, J. Immunol, 2009, 183, 4583–4592. [PubMed: 19752232]
26. Nisapakultorn K, Ross KF and Herzberg MC, Calprotectin expression in vitro by oral epithelial cells confers resistance to infection by *Porphyromonas gingivalis*, Infect. Immun, 2001, 69, 4242–4247. [PubMed: 11401960]
27. Nisapakultorn K, Ross KF and Herzberg MC, Calprotectin expression inhibits bacterial binding to mucosal epithelial cells, Infect. Immun, 2001, 69, 3692–3696. [PubMed: 11349032]
28. Kehl-Fie TE, Zhang Y, Moore JL, Farrand AJ, Hood MI, Rathi S, Chazin WJ, Caprioli RM and Skaar EP, MntABC and MntH contribute to systemic *Staphylococcus aureus* infection by competing with calprotectin for nutrient manganese, Infect. Immun, 2013, 81, 3395–3405. [PubMed: 23817615]
29. Garcia YM, Barwinska-Sendra A, Tarrant E, Skaar EP, Waldron KJ and Kehl-Fie TE, A Superoxide Dismutase Capable of Functioning with Iron or Manganese Promotes the Resistance of Staphylococcus aureus to Calprotectin and Nutritional Immunity, PLoS Pathog., 2017, 13, e1006125. [PubMed: 28103306]
30. Gaddy JA, Radin JN, Cullen TW, Chazin WJ, Skaar EP, Trent MS and Algood HM, Helicobacter pylori Resists the Antimicrobial Activity of Calprotectin via Lipid A Modification and Associated Biofilm Formation, MBio, 2015, 6, e01349–01315. [PubMed: 26646009]
31. Juttukonda LJ, Chazin WJ and Skaar EP, Acinetobacter baumannii Coordinates Urea Metabolism with Metal Import To Resist Host-Mediated Metal Limitation, MBio, 2016, 7.
32. Brophy MB, Nakashige TG, Gaillard A and Nolan EM, Contributions of the S100A9 C-terminal tail to high-affinity Mn(II) chelation by the host-defense protein human calprotectin, J. Am. Chem. Soc, 2013, 135, 17804–17817. [PubMed: 24245608]
33. Makthal N, Nguyen K, Do H, Gavagan M, Chandrangsu P, Helmann JD, Olsen RJ and Kumaraswami M, A Critical Role of Zinc Importer AdcABC in Group A Streptococcus-Host Interactions During Infection and Its Implications for Vaccine Development, EBioMedicine, 2017, 21, 131–141. [PubMed: 28596134]
34. Montgomery RR, Schreck K, Wang X and Malawista SE, Human neutrophil calprotectin reduces the susceptibility of *Borrelia burgdorferi* to penicillin, Infect. Immun, 2006, 74, 2468–2472. [PubMed: 16552081]
35. Posey JE and Gherardini FC, Lack of a role for iron in the Lyme disease pathogen, Science, 2000, 288, 1651–1653. [PubMed: 10834845]

36. Aguirre JD, Clark HM, McIlvin M, Vazquez C, Palmere SL, Grab D, Seshu J, Hart PJ, Saito M and Culotta VC, A Manganese-Rich Environment Supports Superoxide Dismutase Activity in a Lyme Disease Pathogen, *Borrelia burgdorferi*, J. Biol. Chem, 2013, 288, 8468–8478. [PubMed: 23376276]
37. Wang P, Lutton A, Olesik J, Vali H and Li X, A novel iron- and copper-binding protein in the Lyme disease spirochaete, Mol. Microbiol, 2012, 86, 1441–1451. [PubMed: 23061404]
38. Ramsey ME, Hyde JA, Medina-Perez DN, Lin T, Gao L, Lundt ME, Li X, Norris SJ, Skare JT and Hu LT, A high-throughput genetic screen identifies previously uncharacterized Borrelia burgdorferi genes important for resistance against reactive oxygen and nitrogen species, PLoS Pathog., 2017, 13, e1006225. [PubMed: 28212410]
39. Ouyang Z, He M, Oman T, Yang XF and Norgard MV, A manganese transporter, BB0219 (BmtA), is required for virulence by the Lyme disease spirochete, *Borrelia burgdorferi*, Proc. Natl. Acad. Sci. U. S. A, 2009, 106, 3449–3454. [PubMed: 19218460]
40. Troxell B, Xu H and Yang XF, *Borrelia burgdorferi*, a pathogen that lacks iron, encodes manganese-dependent superoxide dismutase essential for resistance to streptonigrin, J. Biol. Chem, 2012, 287, 19284–19293. [PubMed: 22500025]
41. Whitehouse CA, Williams LR and Austin FE, Identification of superoxide dismutase activity in *Borrelia burgdorferi*, Infect. Immun, 1997, 65, 4865–4868. [PubMed: 9353077]
42. Esteve-Gassent MD, Elliott NL and Seshu J, sodA is essential for virulence of *Borrelia burgdorferi* in the murine model of Lyme disease, Mol. Microbiol, 2009, 71, 594–612. [PubMed: 19040638]
43. Bourret TJ, Boylan JA, Lawrence KA and Gherardini FC, Nitrosative damage to free and zinc-bound cysteine thiols underlies nitric oxide toxicity in wild-type *Borrelia burgdorferi*, Mol. Microbiol, 2011, 81, 259–273. [PubMed: 21564333]
44. Bertin PB, Lozzi SP, Howell JK, Restrepo-Cadavid G, Neves D, Teixeira AR, de Sousa MV, Norris SJ and Santana JM, The thermophilic, homohexameric aminopeptidase of *Borrelia burgdorferi* is a member of the M29 family of metallopeptidases, Infect. Immun, 2005, 73, 2253–2261. [PubMed: 15784569]
45. Nguyen KT, Wu JC, Boylan JA, Gherardini FC and Pei D, Zinc is the metal cofactor of *Borrelia burgdorferi* peptide deformylase, Arch. Biochem. Biophys, 2007, 468, 217–225. [PubMed: 17977509]
46. Troxell B and Yang XF, Metal-dependent gene regulation in the causative agent of Lyme disease, Front. Cell. Infect. Microbiol, 2013, 3, 79. [PubMed: 24298449]
47. Troxell B, Ye M, Yang Y, Carrasco SE, Lou Y and Yang XF, Manganese and zinc regulate virulence determinants in *Borrelia burgdorferi*, Infect. Immun, 2013, 81, 2743–2752. [PubMed: 23690398]
48. Vasudevan B and Chatterjee M, Lyme borreliosis and skin, Indian J. Dermatol, 2013, 58, 167–174. [PubMed: 23723463]
49. Neubert U, Krampitz HE and Engl H, Microbiological findings in erythema (chronicum) migrans and related disorders, Zentralbl. Bakteriol. Mikrobiol. Hyg. A, 1986, 263, 237–252. [PubMed: 3577483]
50. Marques A, Schwartz I, Wormser GP, Wang Y, Hornung RL, Demirkale CY, Munson PJ, Turk SP, Williams C, Lee CR, Yang J and Petzke MM, Transcriptome Assessment of Erythema Migrans Skin Lesions in Patients With Early Lyme Disease Reveals Predominant Interferon Signaling, J .Infect. Dis, 2017, 217, 158–167. [PubMed: 29099929]
51. Iotzova-Weiss G, Dziunycz PJ, Freiberger SN, Läuchli S, Hafner J, Vogl T, French LE and Hofbauer GF, S100A8/A9 stimulates keratinocyte proliferation in the development of squamous cell carcinoma of the skin via the receptor for advanced glycation-end products, PLoS One, 2015, 10, e0120971. [PubMed: 25811984]
52. Nukui T, Ehama R, Sakaguchi M, Sonegawa H, Katagiri C, Hibino T and Huh NH, S100A8/A9, a key mediator for positive feedback growth stimulation of normal human keratinocytes, J. Cell. Biochem, 2008, 104, 453–464. [PubMed: 18044712]
53. Thorey IS, Roth J, Regenbogen J, Halle JP, Bittner M, Vogl T, Kaesler S, Bugnon P, Reitmaier B, Durka S, Graf A, Wöckner M, Rieger N, Konstantinow A, Wolf E, Goppelt A and Werner S, The

Ca2+-binding proteins S100A8 and S100A9 are encoded by novel injury-regulated genes, J. Biol. Chem, 2001, 276, 35818–35825. [PubMed: 11463791]

54. Lessard JC, Piña-Paz S, Rotty JD, Hickerson RP, Kaspar RL, Balmain A and Coulombe PA, Keratin 16 regulates innate immunity in response to epidermal barrier breach, Proc. Natl. Acad. Sci. U. S. A, 2013, 110, 19537–19542. [PubMed: 24218583]
55. Leśniak W and Graczyk-Jarzynka A, The S100 proteins in epidermis: Topology and function, Biochim. Biophys. Acta, 2015, 1850, 2563–2572. [PubMed: 26409143]
56. Brandtzaeg P, Dale I and Fagerhol MK, Distribution of a formalin-resistant myelomonocytic antigen (L1) in human tissues. II. Normal and aberrant occurrence in various epithelia, Am. J. Clin. Pathol, 1987, 87, 700–707. [PubMed: 3296737]
57. Wilkinson MM, Busuttil A, Hayward C, Brock DJ, Dorin JR and Van Heyningen V, Expression pattern of two related cystic fibrosis-associated calcium-binding proteins in normal and abnormal tissues, J. Cell Sci, 1988, 91 **(** Pt 2**)**, 221–230. [PubMed: 3267695] **()**
58. Broome AM, Ryan D and Eckert RL, S100 protein subcellular localization during epidermal differentiation and psoriasis, J. Histochem. Cytochem, 2003, 51, 675–685. [PubMed: 12704215]
59. Hughes CA, Kodner CB and Johnson RC, DNA analysis of Borrelia burgdorferi NCH-1, the first northcentral U.S. human Lyme disease isolate, J Clin Microbiol, 1992, 30, 698–703. [PubMed: 1551988]
60. Barbour AG, Isolation and cultivation of Lyme disease spirochetes, Yale J. Biol. Med, 1984, 57, 521–525. [PubMed: 6393604]
61. Zückert WR, Laboratory maintenance of Borrelia burgdorferi, Curr. Protoc. Microbiol, 2007, Chapter 12, Unit 12C 11.
62. Hopkin KA, Papazian MA and Steinman HM, Functional differences between manganese and iron superoxide dismutases in *Escherichia coli* K-12, J. Biol. Chem, 1992, 267, 24253–24258. [PubMed: 1447175]
63. Diaz-Ochoa VE, Lam D, Lee CS, Klaus S, Behnsen J, Liu JZ, Chim N, Nuccio SP, Rathi SG, Mastroianni JR, Edwards RA, Jacobo CM, Cerasi M, Battistoni A, Ouellette AJ, Goulding CW, Chazin WJ, Skaar EP and Raffatellu M, Salmonella Mitigates Oxidative Stress and Thrives in the Inflamed Gut by Evading Calprotectin-Mediated Manganese Sequestration, Cell Host Microbe, 2016, 19, 814–825. [PubMed: 27281571]
64. de Koning J, Histopathologic patterns of erythema migrans and borrelial lymphocytoma, Clin. Dermatol, 1993, 11, 377–383. [PubMed: 8221519]
65. de Carvalho GC, Domingues R, de Sousa Nogueira MA, Calvielli Castelo Branco AC, Gomes Manfrere KC, Pereira NV, Aoki V, Sotto MN, Da Silva Duarte AJ and Sato MN, Up-regulation of Proinflammatory Genes and Cytokines Induced by S100A8 in CD8+ T Cells in Lichen Planus, Acta Derm. Venereol, 2016, 96, 485–489. [PubMed: 26632637]
66. Eming SA, Koch M, Krieger A, Brachvogel B, Kreft S, Bruckner-Tuderman L, Krieg T, Shannon JD and Fox JW, Differential proteomic analysis distinguishes tissue repair biomarker signatures in wound exudates obtained from normal healing and chronic wounds, J. Proteome Res, 2010, 9, 4758–4766. [PubMed: 20666496]
67. Grimbaldeston MA, Geczy CL, Tedla N, Finlay-Jones JJ and Hart PH, S100A8 induction in keratinocytes by ultraviolet A irradiation is dependent on reactive oxygen intermediates, J. Invest. Dermatol, 2003, 121, 1168–1174. [PubMed: 14708622]
68. McGrath JA, Eady RAJ and Pope FM, Rook's Textbook of Dermatology, Blackwell Science Ltd, Malden, MA, 2010.
69. Hsu K, Champaiboon C, Guenther BD, Sorenson BS, Khammanivong A, Ross KF, Geczy CL and Herzberg MC, Anti-Infective Protective Properties of S100 Calgranulins, Antiinflamm. Antiallergy Agents Med. Chem, 2009, 8, 290–305. [PubMed: 20523765]
70. Xu Q, Seemanapalli SV, Reif KE, Brown CR and Liang FT, Increasing the recruitment of neutrophils to the site of infection dramatically attenuates *Borrelia burgdorferi* infectivity, J. Immunol, 2007, 178, 5109–5115. [PubMed: 17404293]
71. Duray PH, Histopathology of clinical phases of human Lyme disease, Rheum. Dis. Clin. North Am, 1989, 15, 691–710. [PubMed: 2685926]

72. Vogl T, Eisenblätter M, Völler T, Zenker S, Hermann S, van Lent P, Faust A, Geyer C, Petersen B, Roebrock K, Schäfers M, Bremer C and Roth J, Alarmin S100A8/S100A9 as a biomarker for molecular imaging of local inflammatory activity, Nat. Commun, 2014, 5, 4593. [PubMed: 25098555]
73. Frosch M, Strey A, Vogl T, Wulffraat NM, Kuis W, Sunderkötter C, Harms E, Sorg C and Roth J, Myeloid-related proteins 8 and 14 are specifically secreted during interaction of phagocytes and activated endothelium and are useful markers for monitoring disease activity in pauciarticular-onset juvenile rheumatoid arthritis, Arthritis. Rheum, 2000, 43, 628–637. [PubMed: 10728757]
74. Wang Y, Zhang Z, Zhang L, Li X, Lu R, Xu P, Zhang X, Dai M, Dai X, Qu J, Lu F and Chi Z, S100A8 promotes migration and infiltration of inflammatory cells in acute anterior uveitis, Sci. Rep, 2016, 6, 36140. [PubMed: 27786310]
75. Costa M, Cruz E, Oliveira S, Benes V, Ivacevic T, Silva MJ, Vieira I, Dias F, Fonseca S, Gonçalves M, Lima M, Leitão C, Muckenthaler MU, Pinto J and Porto G, Lymphocyte gene expression signatures from patients and mouse models of hereditary hemochromatosis reveal a function of HFE as a negative regulator of CD8+ T-lymphocyte activation and differentiation in vivo, PLoS One, 2015, 10, e0124246. [PubMed: 25880808]
76. Pollack RJ, Telford SR, 3rd and Spielman A, Standardization of medium for culturing Lyme disease spirochetes, J. Clin. Microbiol, 1993, 31, 1251–1255. [PubMed: 8501226]
77. Sohnle PG, Hunter MJ, Hahn B and Chazin WJ, Zinc-reversible antimicrobial activity of recombinant calprotectin (migration inhibitory factor-related proteins 8 and 14), J. Infect. Dis, 2000, 182, 1272–1275. [PubMed: 10979933]
78. Linder MC, Ceruloplasmin and other copper binding components of blood plasma and their functions: an update, Metallomics, 2016, 8, 887–905. [PubMed: 27426697]
79. Masuoka J, Hegenauer J, Van Dyke BR and Saltman P, Intrinsic stoichiometric equilibrium constants for the binding of zinc(II) and copper(II) to the high affinity site of serum albumin, J. Biol. Chem, 1993, 268, 21533–21537. [PubMed: 8408004]
80. Waldvogel-Abramowski S, Waeber G, Gassner C, Buser A, Frey BM, Favrat B and Tissot JD, Physiology of iron metabolism, Transfus. Med. Hemother, 2014, 41, 213–221. [PubMed: 25053935]
81. Sohnle PG, Hahn BL and Santhanagopalan V, Inhibition of *Candida albicans* growth by calprotectin in the absence of direct contact with the organisms, J. Infect. Dis, 1996, 174, 1369–1372. [PubMed: 8940237]
82. Stork M, Grijpstra J, Bos MP, Mañas Torres C, Devos N, Poolman JT, Chazin WJ and Tommassen J, Zinc piracy as a mechanism of Neisseria meningitidis for evasion of nutritional immunity, PLoS Pathog., 2013, 9, e1003733. [PubMed: 24204275]
83. Jean S, Juneau RA, Criss AK and Cornelissen CN, Neisseria gonorrhoeae Evades Calprotectin-Mediated Nutritional Immunity and Survives Neutrophil Extracellular Traps by Production of TdfH, Infect. Immun, 2016, 84, 2982–2994. [PubMed: 27481245]
84. Nowakowski AB and Petering DH, Reactions of the fluorescent sensor, Zinquin, with the zinc-proteome: adduct formation and ligand substitution, Inorg. Chem, 2011, 50, 10124–10133. [PubMed: 21905645]
85. Ollig J, Kloubert V, Weßels I, Haase H and Rink L, Parameters Influencing Zinc in Experimental Systems in Vivo and in Vitro, Metals-Basel, 2016, 6.
86. Outten CE and O'Halloran TV, Femtomolar Sensitivity of Metalloregulatory Proteins Controlling Zinc Homeostasis, Science, 2001, 292, 2488–2492. [PubMed: 11397910]
87. Kersten A, Poitschek C, Rauch S and Aberer E, Effects of penicillin, ceftriaxone, and doxycycline on morphology of *Borrelia burgdorferi*, Antimicrob. Agents Chemother, 1995, 39, 1127–1133. [PubMed: 7625800]
88. Alban PS, Johnson PW and Nelson DR, Serum-starvation-induced changes in protein synthesis and morphology of *Borrelia burgdorferi*, Microbiology, 2000, 146 **(** Pt 1**)**, 119–127. [PubMed: 10658658] **()**
89. Lantos PM, Auwaerter PG and Wormser GP, A systematic review of *Borrelia burgdorferi* morphologic variants does not support a role in chronic Lyme disease, Clin. Infect. Dis, 2014, 58, 663–671. [PubMed: 24336823]

90. Meriläinen L, Herranen A, Schwarzbach A and Gilbert L, Morphological and biochemical features of *Borrelia burgdorferi* pleomorphic forms, Microbiology, 2015, 161, 516–527. [PubMed: 25564498]

91. Edgeworth JD, Abiose A and Jones BR, An immunohistochemical analysis of onchocercal nodules: evidence for an interaction between macrophage MRP8/MRP14 and adult *Onchocerca volvulus*, Clin. Exp. Immunol, 1993, 92, 84–92. [PubMed: 8467568]

92. Basika T, Muñoz N, Casaravilla C, Irigoín F, Batthyány C, Bonilla M, Salinas G, Pacheco JP, Roth J, Durán R and Díaz A, Phagocyte-specific S100 proteins in the local response to the *Echinococcus granulosus* larva, Parasitology, 2012, 139, 271–283. [PubMed: 22216900]

93. Marti T, Erttmann KD and Gallin MY, Host-parasite interaction in human onchocerciasis: identification and sequence analysis of a novel human calgranulin, Biochem. Biophys. Res. Commun, 1996, 221, 454–458. [PubMed: 8619876]

94. Gottsch JD, Eisinger SW, Liu SH and Scott AL, Calgranulin C has filariacidal and filariastatic activity, Infect. Immun, 1999, 67, 6631–6636. [PubMed: 10569784]

95. Akpek EK, Liu SH, Thompson R and Gottsch JD, Identification of paramyosin as a binding protein for calgranulin C in experimental helminthic keratitis, Invest. Ophthalmol. Vis. Sci, 2002, 43, 2677–2684. [PubMed: 12147602]

SIGNIFICANCE TO METALLOMICS

All organisms require metal micronutrients such as Zn and Mn to survive. The host exploits this requirement by starving pathogens of these metals using the metal binding protein calprotectin. Here, we provide the first direct evidence that calprotectin can inhibit bacterial growth in the absence of such metal starvation. Specifically, the Lyme disease pathogen *Borreliella (Borrelia) burgdorferi* is sensitive to low doses of calprotectin that inhibit growth by physically interacting with the microbe instead of withholding essential metals. The antimicrobial capacity of calprotectin is indeed complex and mechanisms beyond metal withholding should be considered.

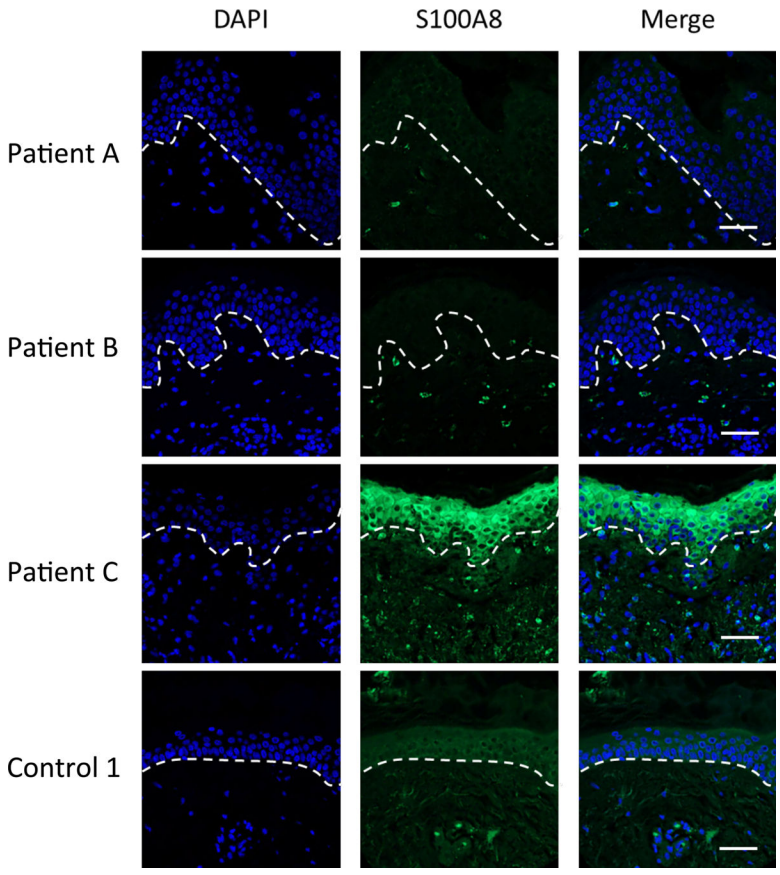

Fig. 1.

Immunofluorescence microscopy imaging of S100A8 expression in the skin of LD patients and controls. Skin tissue sections from the EM rash site of three individual LD patients and one control patient (Control 1) were subjected to immunostaining for S100A8 (green) and nuclei staining with DAPI (blue) before being subjected to fluorescence microscopy at 20× magnification as described in *Experimental*. Dotted lines separate the epidermis from the dermis. Bar represents 50 μm.

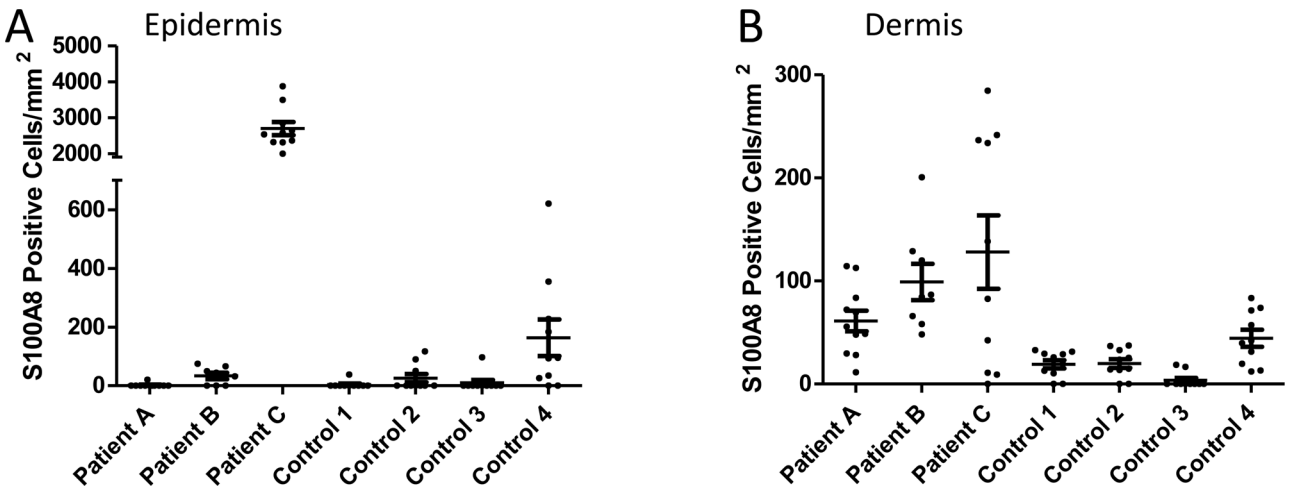

Fig. 2.

Quantification of S100A8 positive cells in the skin of LD patients. S100A8 positive cells were quantified in the epidermis (A) and dermis (B) of skin sections from 3 LD patients and 4 control surgical patients. Results represent cell counts (positive for both DAPI and S100A8) from 8–11 individual images spanning the tissue section of an individual patient. Image numbers: Patient A n=11; patient B n=8; patient C and all four controls n=10. (A) S100A8 staining in the epidermis of patient A is significantly higher than all four controls ($p < 0.001$) and individual patients B and C ($p<0.001$). (B) S100A8 staining in the dermis of patient C is significantly higher than all four controls ($p < 0.01$); the same is true for patient B and controls 1–3 ($p<0.05$).

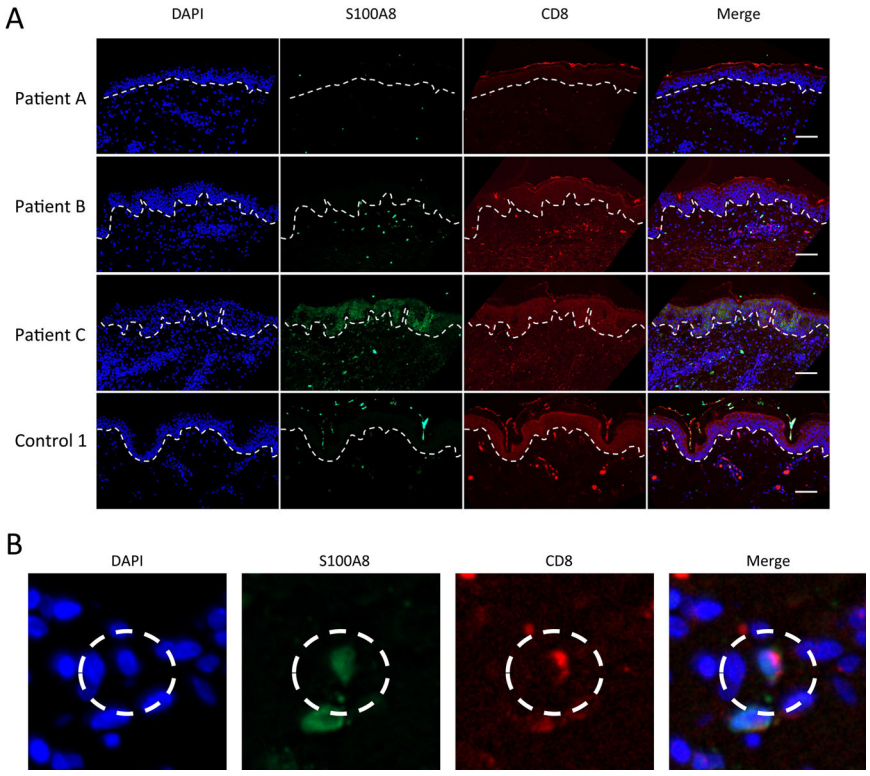

Fig. 3.

Co-localization of S100A8 and CD8 expression in the dermis. (A) Skin tissue sections from the EM rash site of three individual LD patients and one control (control 1) were subjected to immunostaining for S100A8 (green), CD8 (red) and nuclei staining with DAPI (blue) before being subjected to fluorescence microscopy at 20× magnification as in Fig. 1. Dotted lines separate the epidermis from the dermis and bar represents 50 μm. (B) Individual cells co-expressing S100A8 and CD8 were identified by staining with anti-S100A8 (green), anti-CD68 (red) and DAPI (blue) as shown in the dotted circle.

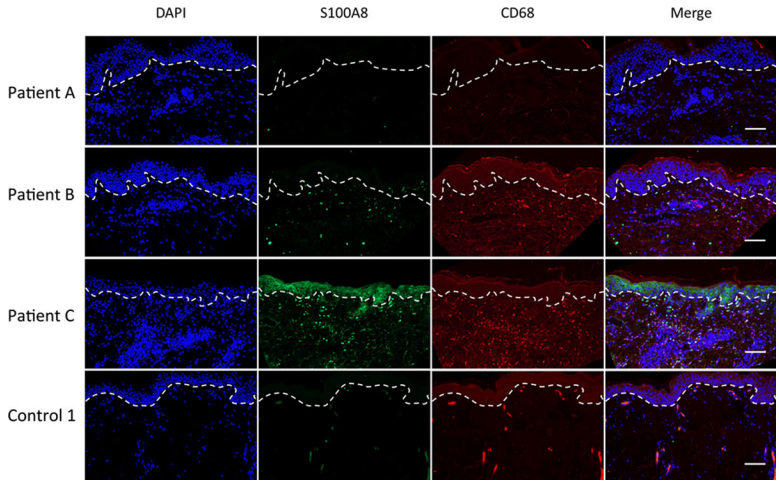

Fig. 4.

Expression of S100A8 and CD68 expression in the dermis. Skin tissue section from the EM rash site of three individual LD patients and one control were subjected to immunostaining for S100A8 (green), CD68 (red) and nuclei staining with DAPI (blue) before being subjected to fluorescence microscopy at 20× magnification as in Fig. 1. Dotted lines separate the epidermis from the dermis and bar represents 50 μm.

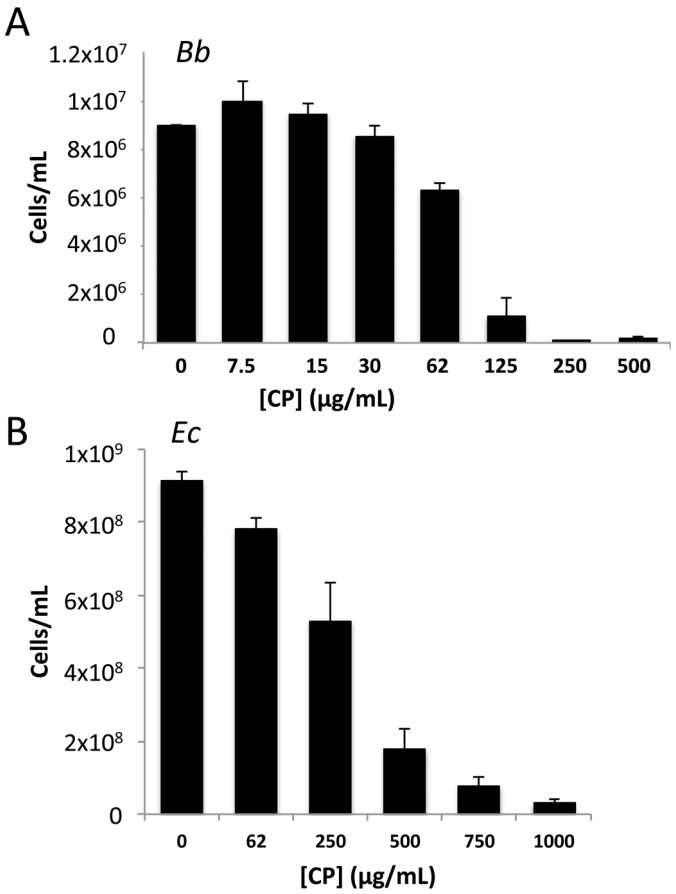

Fig. 5.

Calprotectin (CP) mediated growth inhibition of *B. burgdorferi* (*Bb*) versus *E. coli. Bb* (A) or *E. coli* (B) were cultured in BSK II medium as described in *Experimental* in the presence of the indicated concentrations of CP. (A) *Bb* cell number was enumerated under dark field microscopy; results are averages of three biological replicates representative of seven experimental trials. There was essentially no growth at 250 and 500 μg/mL CP and the cell number approximated the original inoculum. (B) *E. coli* cell number was converted from optical density; results are the averages of four biological replicates and are representative of eight experimental trials. Error bars are standard error. Across numerous experimental trials, the mean inhibitory concentration or dose of CP that inhibits growth by 50% for *Bb* and *E. coli* were ≈80 and ≈350 μg/mL, respectively.

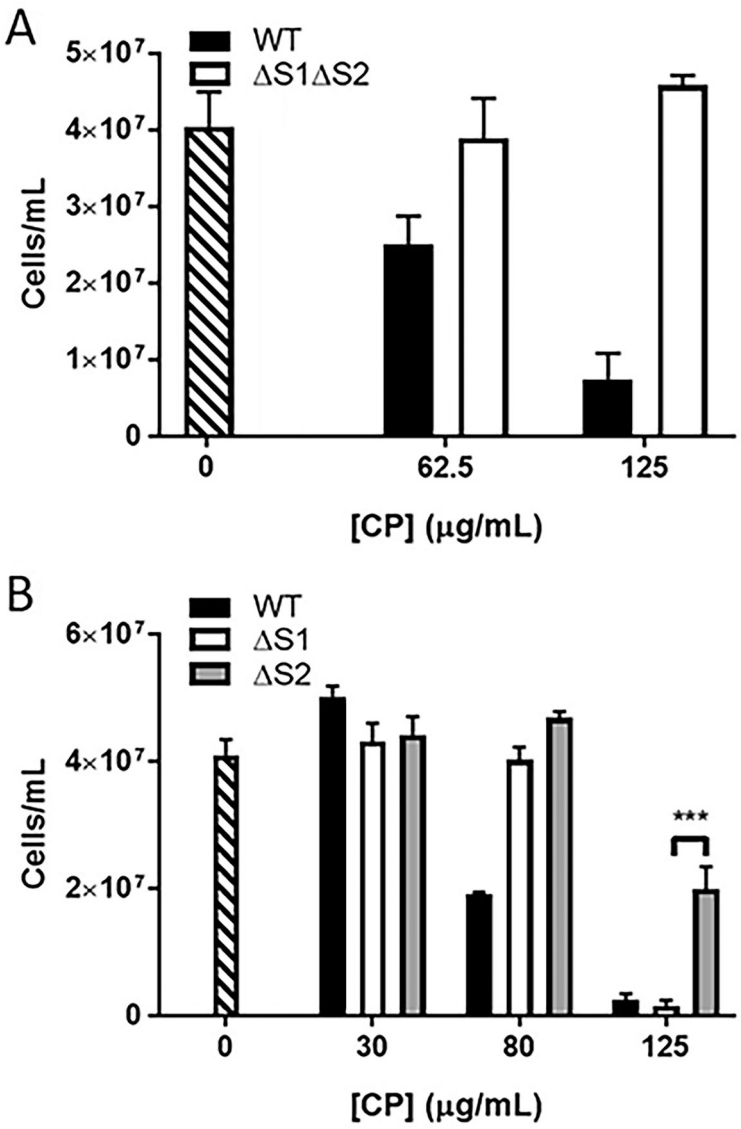

Fig. 6.

Effect of CP metal binding mutants on inhibiting growth of *Bb*. *Bb* cells were grown as in Fig. 5A in the presence of WT CP (black bar), the indicated metal binding mutants of CP (white and grey bars), or without CP (stippled bar). Results are averages of three biological replicates and are representative of five (A) and three (B) experimental trials; error bars are standard error. The difference in growth inhibition between ΔS1 and ΔS2 CP at 125 μg/mL is statistically significant; ***p = 0.001.

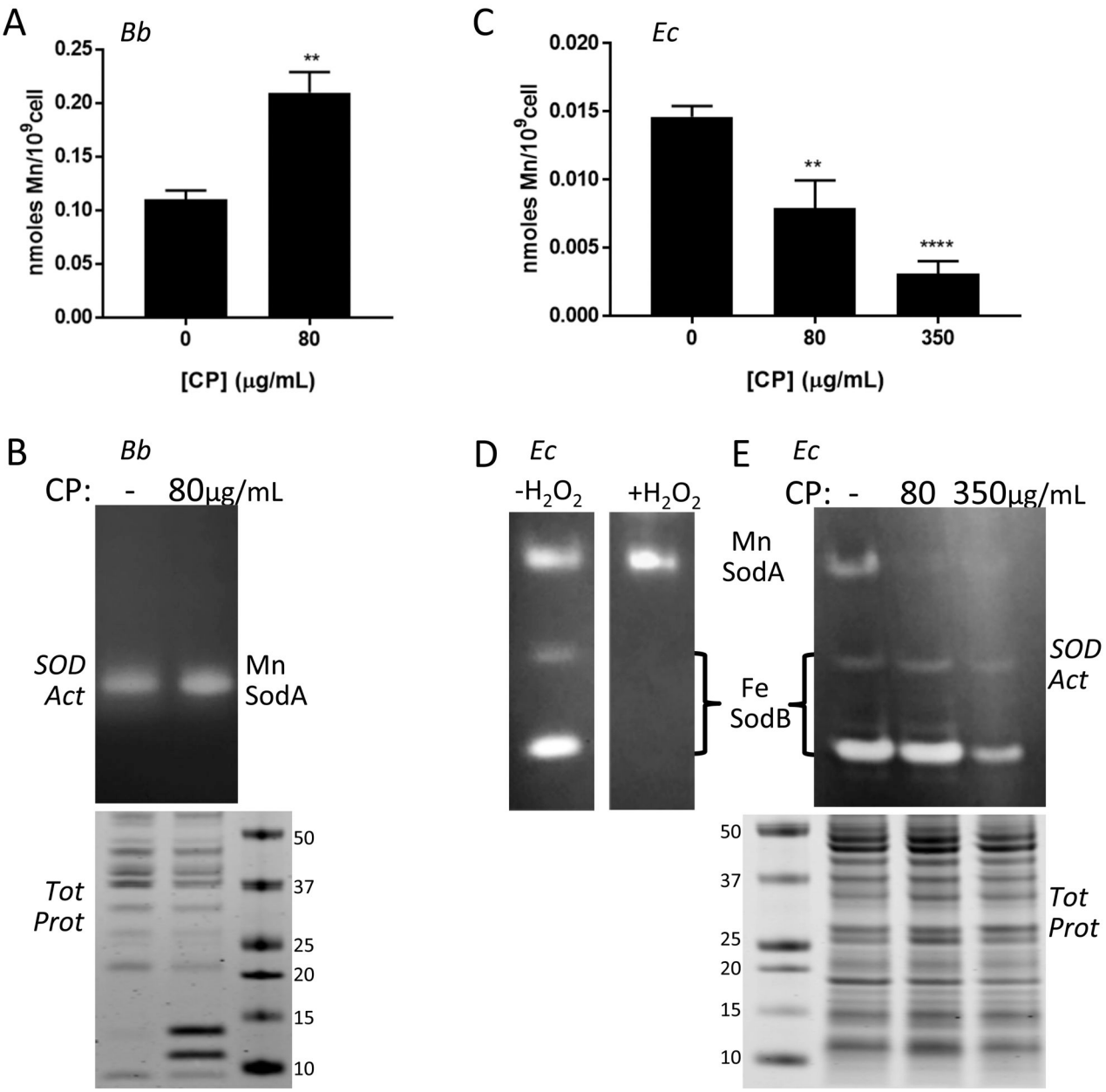

Fig. 7.

Effects of CP on Mn requiring SodA and total cellular Mn in *Bb* versus *E. coli*. *Bb* (A, B) and *E. coli* cells ("*Ec*" C-E) were grown in BSK II supplemented with the designated concentrations of CP. (A,C) Mn levels were measured in *Bb* (A) or *E. coli* (C) cells by ICP-MS. Results are averages of at least five (A) and four (C) replicates over three experimental trials, **$p \leq 0.0035$, ****$p < 0.0001$, where CP treated samples are compared to no CP controls. Error bars are standard error. (B,D,E) Whole cell lysates were analyzed for SOD enzymatic activity by native gel electrophoresis and NBT staining (B top, D, E top). Denaturing gel electrophoresis and coomassie staining (B bottom, E bottom) were used as a loading control. The positions of SodA and SodB on the native gels are indicated; numbers represent molecular weight markers. Results are representative of five (B) and three (E)

experimental trials. (D) The native gel was treated with H_2O_2 where indicated to inactivate Fe containing SodB prior to NBT staining, as described in *Experimental*.

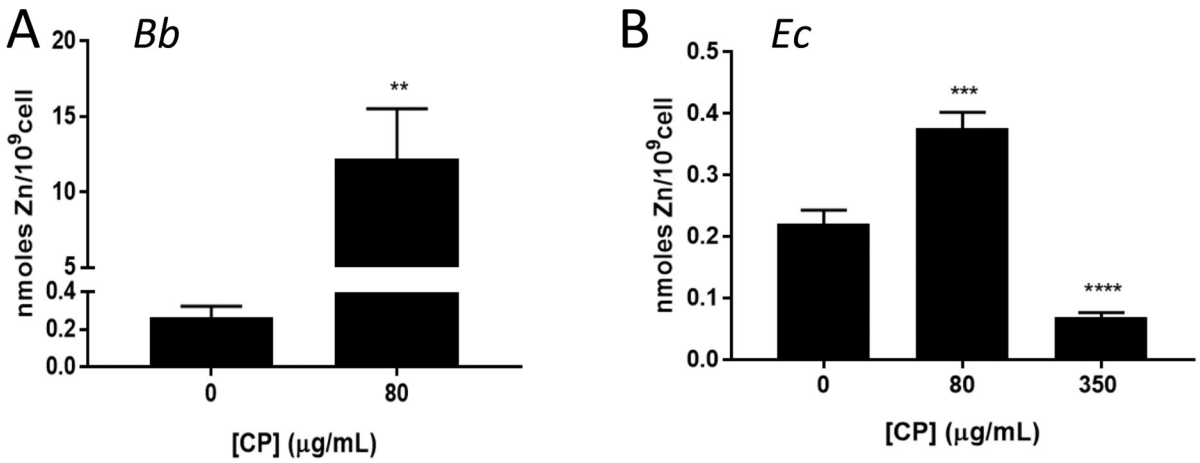

Fig. 8.

Zn and CP in *Bb* versus *E. coli*. Total Zn levels were measured by ICP-MS in whole cell samples of *Bb* or *E. coli* grown with the indicated concentration of CP. (A) Results are averages of eight (0 μg/mL CP) and eleven (80 μg/mL CP) replicates over five independent experiments, where the level of Zn in CP treated cell samples ranged from ≈6–30 nmoles/109 cells; **p=0.0073. (B) Results are averages of 10 (0 μg/mL CP), 8 (80 μg/mL CP), and 7 (350 μg/mL CP) replicates over four experimental trials, ***p=0.0004; ****p<0.0001.

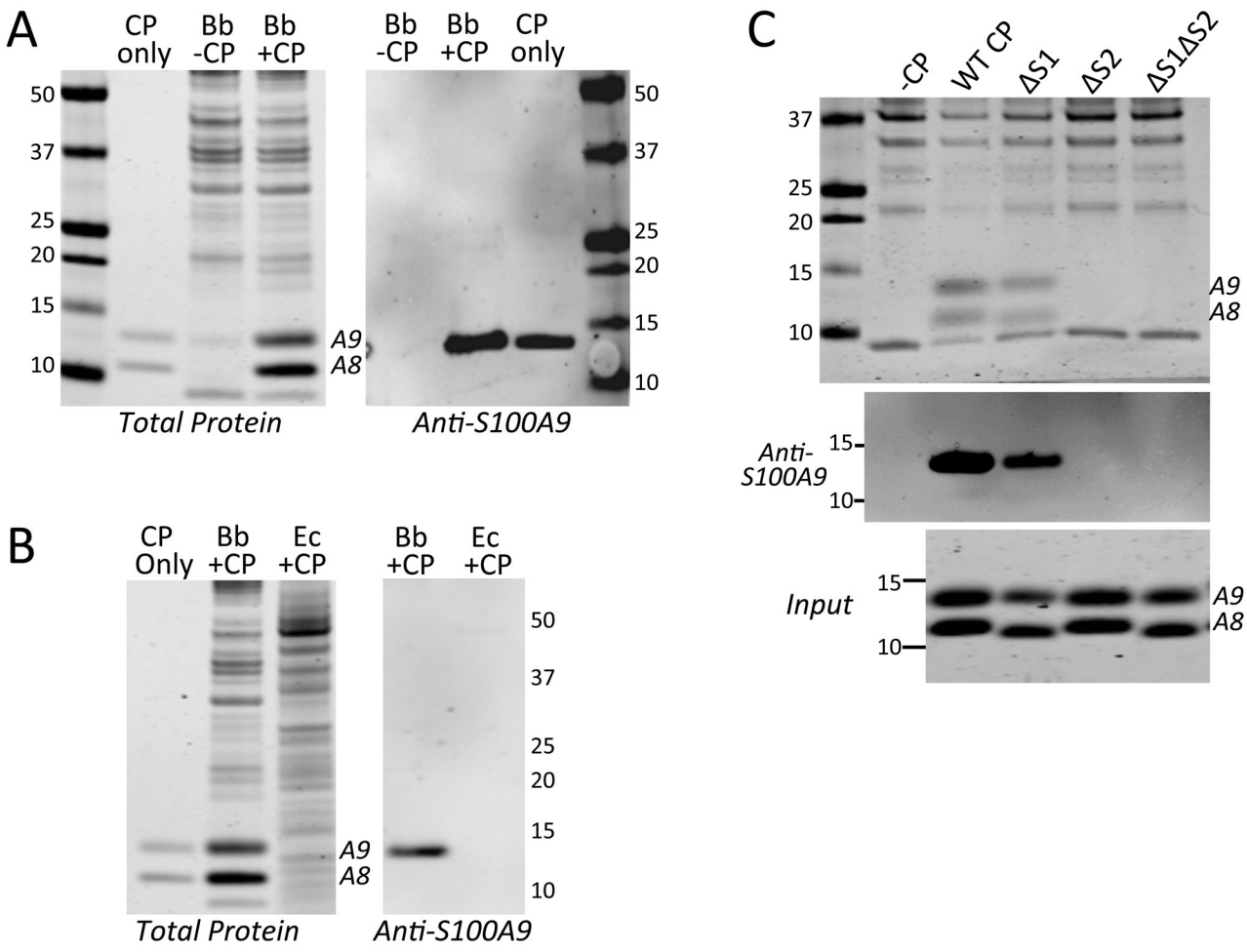

Fig. 9.

Interactions between CP and *Bb*. *Bb* or *E. coli* cells were grown in BSK II in the absence or presence of 80 or 350 μg/mL CP, (A, B). *Bb* was grown with 80 μg/mL of the designated CP mutants (C). Whole cell lysates were subjected to denaturing gel electrophoresis and either coomassie staining for total protein (A,B left, C top) or immunoblot analysis for S100A9 ("Anti-S100A9"). "CP only" is 500 ng of recombinant human CP. Numbers indicate molecular weight markers and positions of S100A8 and S100A9 are denoted. "Input" shows coomassie staining of WT and the indicated CP mutants added to *Bb* cultures. Over five experimental trials, the level of ΔS1 CP recovered in *Bb* lysates (as in Fig. 9C top and middle panels) was 42% (± 12%) that of WT CP, while ΔS2 and ΔS1ΔS2 CP were undetected.

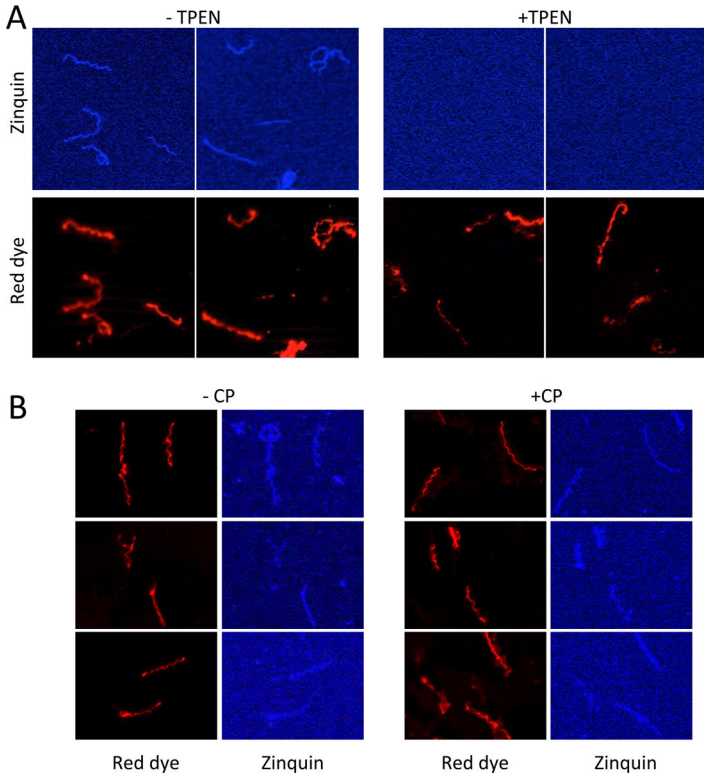

Fig. 10.

Zinquin labeling of *Bb*. *Bb* cells were cultured in the absence (A, left) or presence (A, right) of 3 μM TPEN, a Zn chelator, or in the absence (B, left) or presence (B, right) of 80 μg/mL CP. Cells were prepared for fluorescence microscopy by sequential staining with zinquin and then PKH red dye (for membranes) as described in *Experimental*. Results are representative of 10 (A) and 20 (B) images.

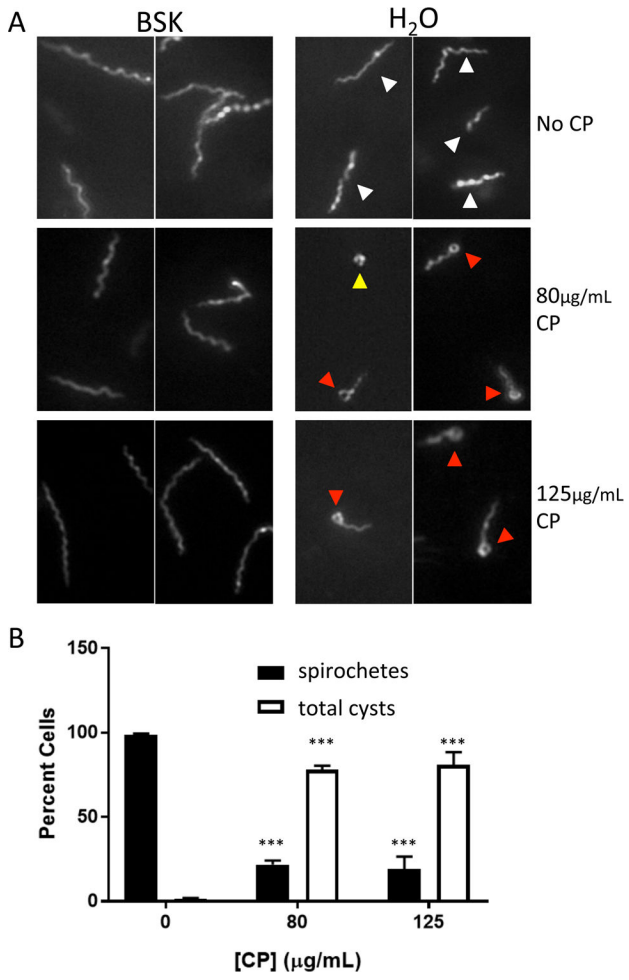

Fig. 11:

CP and morphology of *Bb*. (A) *Bb* cells cultured with the indicated concentrations of CP were examined by dark field microscopy either directly in BSK II medium or immediately following a 1:10 dilution in H_2O. Arrows indicate morphology classes: white, elongated spirals; red, cysts with round body tip; yellow, full round body cysts. Similar results were obtained with 1:5 dilution in H_2O (Fig. S5, ESI†). (B) Quantification of cell morphology following dilution in H_2O. Cysts are a combination of the two classes described above where full round bodies are less <5% total cysts. Results represent the averages of >250 cells counted over 3–4 experimental trials. Error bars are standard error. The changes in morphology with 80 and 125 μg/mL CP compared to no CP are statistically significant; ***$p<0.001$

TABLE 1

Dermal cells positive for S100A8 and CD8

Sample[1]	S100A8+[2]	CD8+[2]	CD8+/S100A8+[3]
Patient A	147	46	21
Patient B	30	6	1
Patient C	76	6	1
Control 1	1	4	1
Control 2	7	1	0
Control 3	0	0	0
Control 4	19	1	1

[1] LD patient number or four individual controls/non-LD patients

[2] Total S100A8 or CD8 counted in two individual sections of patient C and a single section from the remaining patients and controls.

[3] Number of cells that co-stained with S100A8 and CD8

TABLE 2

Dermal cells positive for S100A8 and CD68

Sample[1]	S100A8+[2]	CD68+[2]	CD68/S100A8+[3]
Patient A	102	59	40
Patient B	18	1	0
Patient C	202	78	48
Control 1	3	6	2
Control 2	9	7	3
Control 3	2	1	1
Control 4	13	0	0

[1] LD patient number or four individual controls/non-LD patients

[2] Total S100A8 or CD68 counted in two individual sections of patient A and a single section from the remaining patients and controls.

[3] Number of cells that co-stained with S100A8 and CD68